

1 **Retrieval of Snow Properties for Ku- and Ka-band Dual-Frequency Radar**

2

3

4

5 Liang Liao¹, Robert Meneghini², Ali Tokay³ and Larry F. Bliven⁴

6

7 ¹ Goddard Earth Science Technology & Research, Morgan State University, MD

8 ² NASA Goddard Space Flight Center, Greenbelt, MD

9 ³ University of Maryland Baltimore County/JCET, MD

10 ⁴ NASA Wallops Flight Facility, VA

11

12

13 Submitted to

14 Journal of Applied Meteorology and Climatology

15

16

17

18 Corresponding author information:

19

20 Dr. Liang Liao
21 Goddard Earth Sciences Technology and Research
22 Morgan State University
23 Code 612
24 NASA/Goddard Space Flight Center
25 Greenbelt, MD 20771

26

27 301-614-5718 (phone)

28 301-614-5492 (fax)

29 Email: Liang.Liao-1@nasa.gov

30

31

Abstract

32 The focus of this study is on the estimation of snow microphysical properties and the associated
33 bulk parameters such as snow water content and water equivalent snowfall rate for Ku- and Ka-
34 band dual-frequency radar. This is done by exploring a suitable scattering model and the proper
35 particle size distribution (PSD) assumption that accurately represent, in the electromagnetic
36 domain, the micro/macro-physical properties of snow. The scattering databases computed from
37 simulated aggregates for small to moderate particle sizes are combined with a simple scattering
38 model for large particle sizes to characterize snow scattering properties over the full range of
39 particle sizes. With use of the single scattering results, the snow retrieval look-up tables can be
40 formed in a way that directly links the Ku- and Ka-band radar reflectivities to snow water
41 content and equivalent snowfall rate without use of the derived PSD parameters. A sensitivity
42 study of the retrieval results to the PSD and scattering models is performed to better understand
43 the dual-wavelength retrieval uncertainties. To aid in the development of the Ku- and Ka-band
44 dual-wavelength radar technique and to further evaluate its performance, self-consistency tests
45 are conducted using measurements of the snow PSD and fall velocity acquired from the Snow
46 Video Imager/Particle Image Probe (SVI/PIP) during the winter of 2014 in the NASA Wallops
47 flight facility site in Wallops Island, Virginia.

48

49 **1 Introduction**

50
51 The Global Precipitation Measurement (GPM) core satellite, a joint Earth-observing mission
52 between the National Aeronautics and Space Administration (NASA) and the Japan Aerospace
53 Exploration Agency (JAXA), was successfully launched into orbit on 27 February of 2014 from
54 Japan (Hou et al. 2008 and 2014). One of the goals of the Dual-frequency Precipitation Radar
55 (DPR) aboard the GPM satellite is to provide measurements and estimates of snow precipitation
56 rate and water content for mid- and high-latitude regions. This is usually done by estimating
57 parameters of snow particle size distribution (PSD) that are often modeled by an analytical
58 function, such as the exponential, gamma or lognormal distribution, with two or three unknown
59 parameters (Gorgucci et al. 2000 and 2002; Bringi et al. 2002). The inability of the modeled PSD
60 to represent actual snow spectra and to characterize their intrinsic variations in time and space
61 can lead to errors in the estimates of precipitation rate obtained from the DPR. Additionally,
62 uncertainties associated with scattering computations of snow aggregates also affect the accuracy
63 of the dual-wavelength radar retrieval of snow arising from the complex shape and structure of
64 snow aggregates and the corresponding variability in the scattering parameters. Therefore,
65 understanding the uncertainties in snow precipitation estimation that depend on PSD
66 parameterizations and scattering models of individual particles is important in evaluating the
67 overall performance of DPR retrieval algorithms and in gaining insight into ways to improve the
68 algorithms.

69
70 Several studies have been carried out using dual-frequency radar for the retrieval of precipitating
71 ice/snow parameters from the ground (Matrosov 1998; Szyrmer and Zawadzki 2014) and from
72 airborne radar measurements (Liao et al. 2005, 2008; Heymsfield et al. 2005; Wang et al. 2005;

73 Matrosov et al. 2005). Although various combinations of frequencies were used in these studies,
74 a common feature is that at least one of the radar frequencies operates in the non-Rayleigh
75 regime to ensure a measurable difference in the reflectivities. It is this differential reflectivity
76 that can be related to a characteristic size parameter of the snow particle distribution. Because
77 of uncertainties in the snow microphysics arising from the natural variability of the particle
78 density, shape, and orientation and also because of uncertainties associated with the particle
79 backscattering cross section and terminal fall velocity as well as the natural variability in PSDs,
80 it is important to assess the errors in the model and their impacts on the retrievals.

81

82 The emphasis of this study is on the estimation of snow microphysical properties and the
83 associated bulk parameters such as snow water content and water equivalent snowfall rate. As
84 indicated earlier, one of the challenges in the radar retrieval of snow is to characterize the
85 variability of the snow PSD and to efficiently compute scattering properties of the snowflakes
86 over the full range of sizes. The aim of our study is to explore a suitable scattering model and an
87 appropriate PSD that accurately represents, in the electromagnetic domain, the micro/macro-
88 physical properties of snow.

89

90 Although several scattering databases are available, which provide the scattering properties of
91 snow aggregates (Liu 2004 and 2008; Nowell et al. 2013; Kuo et al. 2016), they are often limited
92 to small-to-moderate particle sizes for a limited set of frequencies. These limitations arise not
93 only because of the magnitude of the computational burden but also because of the convergence
94 properties of the numerical solution. To develop an operational-type radar algorithm for the DPR
95 snow retrieval, it is desirable to have a scattering model that provides efficient computation at an

96 arbitrary frequency over a large range of particle sizes. Comparisons of the scattering results
97 between simple and more complicated snow models indicate that the scattering properties of
98 aggregates at the DPR frequencies are fairly well reproduced by randomly-oriented ellipsoidal
99 particles if the effective mass density of snow is constant with size (Liao et al. 2013). By taking
100 advantage of both developed scattering databases and simple scattering models, we attempt to
101 employ the scattering results of the aggregates from the scattering database for small to moderate
102 particle sizes and use the results from the simple scattering models for large particles to cover the
103 full range of particle sizes for characterizing snow scattering properties at Ku- and Ka-band.

104

105 One of the DPR algorithms for snow retrieval employs a fixed-snow-density spherical model for
106 computations of the Ku- and Ka-band radar backscattering and extinction cross sections using
107 the assumption of an exponential PSD (Seto et al. 2013). To improve snow retrieval accuracy,
108 we will investigate retrieval uncertainties associated with the PSD and the particle scattering
109 models, and introduce new forms of the retrieval look-up tables that directly link DPR Ku- and
110 Ka-band radar reflectivities to snow water content and snowfall rate without the use of derived
111 PSD parameters. Newly formed look-up tables provide an effective means not only for snow
112 retrieval but for analysis of the retrieval uncertainties associated with the PSD model and the
113 particle scattering models. In order to check the consistency of the snow retrievals,
114 measurements of the snow PSD and fall velocity acquired from the Snow Video Imager/Particle
115 Image Probe (SVI/PIP) are used (Newman et al. 2009). It is believed that a collection of long-
116 term PSD data, fall velocities and information on particle mass spectra will provide a strong
117 basis for evaluating the performance of the DPR Ku- and Ka-band techniques.

118

119 This article is organized as follows. Methods for snow retrieval are described in Section 2, and
120 measurements of the PSD are discussed in Section 3, followed by remarks and a summary in
121 Section 4.

122

123 2 Technical Approach and Methodology

124

125 Understanding the retrieval errors associated with the snow particle size/mass distributions
126 models and particle scattering models employed by the DPR algorithms is important for the
127 evaluation of algorithm performance. The study also provides insight into which of the models
128 yield the most accurate DPR estimates of snow. Proper selection of the PSD and scattering
129 models can improve the overall performance of the DPR profiling algorithm. What follows are
130 discussions of snow scattering models and the parameterization of the particle size spectra and
131 how these models affect the radar retrievals.

132

133 2.1 Single scattering model of snow aggregates

134

135 Several simulated aggregate models have been developed using the pristine ice crystal habits
136 found in nature as the basic elements from which the aggregates are constructed (Draine and
137 Flatau 1994; Liu 2004 and 2008; Weinman and Kim 2007; Petty and Huang 2010; Botta et al.
138 2010 and 2011; Nowell et al. 2013; Kuo et al. 2016). For these particles, a numerical scheme is
139 required to compute the scattered fields. Although these numerical computations are useful, they
140 are time consuming, and are often limited to small-to-moderate particle sizes for a limited set of
141 frequencies. A few scattering databases derived from simulated aggregates are available (Nowell
142 et al. 2013; Kuo et al. 2016), but the maximum equivalent ice diameter is limited to around 2.5-3
143 mm which is not large enough to cover entire particle size range.

144
145 To account for the scattering contribution from the entire particle size range, the current DPR
146 algorithms adopt a simple scattering model, namely, the ice-air mixed spheres with a fixed snow
147 density of 0.1 g/cm^3 for all particle sizes (Seto et al. 2013). To check the validity and accuracy of
148 the simple geometric scattering model, a study was carried out by Liao et al. (2013) in which
149 scattering results from aggregates comprised of 6-branch bullet rosette crystals were compared
150 with those obtained from spherical or spheroidal ice-air mixed phase particles. Shown in Fig.1 is
151 an example of these results, in which backscattering (left) and extinction (right) coefficients at
152 35.6 GHz are plotted versus the equivalent ice diameter for 3 simulated snow aggregates and
153 results from the sphere, oblate and prolate spheroids. A constant effective snow density of 0.2
154 g/cm^3 is assumed for all spherical and spheroidal particle models. The spheroids are assumed to
155 be randomly oriented, i.e., their symmetry axes are uniformly distributed in three-dimensional
156 space. The aspect ratios (γ) of the spheroids, defined as the ratio of polar to equatorial lengths,
157 are taken to be either 0.5 or 2 to represent oblate and prolate spheroids respectively. The results
158 of the study show that the scattering properties of the aggregates are fairly well reproduced by an
159 equivalent-mass spheroidal particle when a constant snow density is assumed.
160
161 Agreement between the spheroidal/fixed density model and the aggregates suggests the validity
162 of the simple model and its utility for computing look-up tables for the DPR. An effective snow
163 density of 0.2 g/cm^3 is best able to reproduce the scattering parameters of the bullet-rosette
164 aggregates at the DPR frequencies. It is important to note that the effective mass density, as
165 defined in this paper, is that mass density of a spheroidal particle whose associated scattering
166 parameters provide the best match to those of the simulated aggregates with the same mass. This
167 definition is motivated by the desire to match the scattering properties of the spheroidal and

168 simulated aggregates and is distinct from the usual definition of snow density given by the ratio
169 of the particle mass to the volume where the volume is taken to be that of a circumscribing
170 sphere or spheroid. To distinguish our definition from others, the density we use for scattering
171 computations is referred to as the effective snow density. It is also important to note that the
172 snow mass is preserved in both definitions; that is, the product of the mass density or effective
173 mass density and the particle volume yields the same mass.

174

175 Recently, Kuo et al. (2016) have developed a comprehensive scattering database, which is
176 computed using the discrete dipole approximation (DDA) from a collection of realistic
177 aggregates simulated from a 3-D growth model with mass vs. size and fractal properties that are
178 consistent with field observations (Gravner and Griffeath 2009). Because of its limited range of
179 particle size mentioned earlier, the scattering tables of snow aggregates in our study will be taken
180 as a hybrid form that combines the scattering results from the Kuo et al. scattering database for
181 small to moderate particle sizes and the results from the simple scattering models for large
182 particles. Illustrated in Figs.2 and 3 are these scattering results at Ku- and Ka-bands from the
183 Kuo et al. database along with the results from an oblate spheroidal model for particle diameters
184 up to 6 mm. The results from the simple models (red curves) are those obtained from the
185 randomly-oriented oblate spheroids with an aspect ratio of 0.7 and a constant effective mass
186 density of 0.2 g/cm^3 . The results of the scattering tables, which are denoted by the term “fitted”
187 and shown by the black curves, represent the mean values of the data from the scattering
188 database, where the mean is taken from all types of aggregates having the same mass, and the
189 results from the 0.2 g/cm^3 oblate spheroid model in the size range where the scattering database
190 is unavailable. The maximum liquid equivalent diameters of the current Kuo et al. database at

191 Ku- and Ka-bands are 3 and 2 mm, respectively. In other words, the scattering results from the
192 simple models are employed in the tables for the size ranges from 3-6 mm at Ku-band and 2-6
193 mm at Ka-band. The fairly good agreement of the scattering results in Figs. 2 and 3 between the
194 simple model and the scattering database (with mean differences less than 10% for the
195 backscattering and 7% for extinction cross sections) over the size range where the database is
196 valid suggests the validity of the simple models for the smaller particle sizes. As the scattering
197 database is updated to cover larger particle sizes, the validity of the simple scattering model will
198 be reassessed.

199

200 2.2 Particle size/mass distribution model

201

202 The three-parameter gamma distribution is one of the most common ways to mathematically
203 describe hydrometeor size/mass distributions (Gorgucci et al. 2000 and 2002; Bringi et al. 2002).
204 The form of the gamma distribution is expressed as

205

$$N(D) = N_w f(\mu) \left(\frac{D}{D_m} \right)^\mu \exp(-\Lambda D), \quad (1)$$

206 where D_m is the mass-weighted diameter of the particle, N_w is a scale factor, and μ is the shape
207 factor where

208

$$f(\mu) = \frac{6(4 + \mu)^{\mu+4}}{4^4 \Gamma(\mu + 4)} \quad \text{and} \quad \Lambda = (4 + \mu)/D_m, \quad (2)$$

209 To describe snow particle size and mass spectra, the PSD in (1) and (2) is given as a function of
210 liquid equivalent or melted diameter D , which is also called particle melted-size distribution. D_m
211 is the melted median mass diameter, defined by

212

213

$$D_m = \frac{\int_0^{\infty} D^4 N(D) dD}{\int_0^{\infty} D^3 N(D) dD}. \quad (3)$$

214

215 In the inner swath, the DPR provides Ku- and Ka-band reflectivity factor measurements at each
 216 range gate so only two parameters of the PSD can be determined. Typically, the shape factor (μ)
 217 is taken to be constant. Although μ is often set to zero (exponential distribution) (Gunn and
 218 Marshall 1958; Seto et al. 2013), the impact of this choice on the retrieval needs to be
 219 investigated.

220

221 The differential frequency ratio (DFR), which is defined as the difference between the radar
 222 reflectivity factors at Ku- and Ka-bands in decibels, is perhaps the most important quantity for
 223 the dual-wavelength radar techniques in estimating hydrometeor micro/macro-physical
 224 properties. As the DFR is independent of N_w , D_m can be derived from the DFR relations once μ
 225 has been fixed. However, the DFR- D_m relation depends not only on μ but on the particle shape,
 226 orientation distribution and mass density. Fig.4 provides the results of DFR as a function of the
 227 liquid equivalent median mass diameter using a randomly-oriented, fixed density spheroidal
 228 particle model. The left plot shows the variations in the DFR- D_m relation resulting from
 229 different effective snow densities. Computations of the radar scattering parameters at different
 230 effective snow densities are made in the same way as in the case of 0.2 g/cm³. The particle sizes
 231 (semi axes of spheroid) are solely determined by the density specified for a given particle mass.
 232 The center plot shows the effects of particle shape where a γ value of 1 corresponds to a sphere
 233 while γ values less than 1 correspond to an oblate spheroid. The plot on the right shows the
 234 effect of changing μ . Analysis of these results indicates that particle shape has a small effect on

235 the DFR- D_m relation and changes the results by less than 4% for changes in γ from 0.5 to 1 while
236 the shape factor leads to the change in the results of no more than 20%. On the other hand, the
237 DFR- D_m relation has a strong dependence on the effective snow density. In other words, the
238 determination of D_m from the DFR is relatively insensitive to μ and to particle shape, if the
239 orientation is random, whereas the relationship is quite sensitive to the effective snow density
240 used for computations of the scattering parameters. As can be seen in Figs.1-3, the extinction
241 coefficients at both Ku- and Ka-bands, though in good agreement between the simple model and
242 the scattering database, are small and can usually be neglected. It should be noted that the above
243 conclusions are based on the assumption of random orientation of the aggregates. When this
244 assumption is violated, then the orientation distribution as well as particle shape become
245 important.

246

247 Although an effective snow density of 0.2 g/cm^3 is found to be suitable for the computations of
248 the Ku- and Ka-band radar scattering parameters for equivalent ice diameters up to 2-3 mm,
249 further testing will be necessary to assess this assumption when scattering results from larger
250 aggregates become available. It is worth noting that the results of Liao et al. (2013) show
251 reasonably good agreement between radar scattering parameters at higher frequencies (from 89-
252 183.31 GHz) as derived from the simple models and the simulated aggregates for particle
253 diameters up to 2.5 mm despite the fact that the simple models using spheres or nearly spherical
254 particles produce backscattering results with more pronounced oscillations (resonance effects)
255 than the aggregate results. This is encouraging in the sense that it shows that an effective density
256 of 0.2 g/cm^3 yields good agreement with the simulated aggregate results for electrically larger
257 particles. On the other hand, it might be the case that the effective snow density may need to be

258 changed for larger particle types so as to ensure good agreement. In either case, the objective is
259 to provide scattering tables at all relevant frequencies and particle sizes that incorporate the most
260 recent scattering results.

261

262 2.3 Dual-wavelength retrieval algorithm

263

264 As discussed above, D_m can be derived from the DFR- D_m relations for a given μ . In principle,
265 once D_m is determined, N_w is derived using the radar reflectivity at either Ku- or Ka-band.
266 Subsequently, snow water content (SWC) and equivalent snowfall rate (R_s) can be computed
267 from the derived PSD parameters. The fall velocity of snow is needed in order to estimate R_s .
268 For the development of an effective dual-wavelength radar retrieval technique, it is desirable to
269 employ look-up tables (LUT) that are formed in such a way that the radar measurements are
270 directly linked to the microphysical properties of snow (D_m and N_w) and its associated bulk
271 parameters (SWC and R_s). With use of the LUTs different particle models and their scattering
272 properties can be evaluated separately in the context of the same algorithm.

273

274 Illustrated in Fig.5 are such tables in which SWC (top-left), R_s (top-right), D_m (bottom-left) and
275 N_w (bottom-right) along the ordinate are given as a function of the DFR. A flowchart is provided
276 in Fig.6 showing the procedures to compute the radar reflectivity factors and snow size and
277 bulk hydrometeor parameters from an assumed mass spectrum model. In Fig.5, SWC, R_s , N_w
278 have been normalized by the Ku-band radar reflectivity factor so that they can be expressed
279 solely as a function of DFR for given PSD and scattering models. The way to normalize liquid
280 water content by reflectivities has previously been adopted in the study of ice clouds (Hogan et

281 al. 2000; Botta et al. 2013). The results in Fig.5 are computed under the assumption that the
282 snow particles are fixed-density, randomly-oriented oblate spheroids with an aspect ratio of 0.7
283 that follow an exponential particle size distribution. As an example, and also for reference, the
284 tables are plotted in Fig.5 for effective snow densities varying from 0.05 to 0.5 g/cm³. The
285 terminal velocities of snowflakes used for the computations of R_S are based on the results of
286 Magono and Nakamura (1965). It is important to note that the results from the LUTs shown in
287 Fig.5 can be used to determine SWC and R_S as they directly link the DPR radar reflectivities to
288 SWC and R_S without use of the derived PSD parameters.

289

290 The procedure for the estimation of snow parameters is described as follows: given a pair of
291 reflectivity factors (Z_{Ku} , Z_{Ka}), the DFR in dB is defined as $10\log_{10}(Z_{Ku}/Z_{Ka})$, from which we find
292 the values of SWC/Z_{Ku} (left) and R_S/Z_{Ku} (right) for an assumed effective snow density. By
293 multiplying by Z_{Ku} , the results of SWC and R_S are then obtained. Obviously the values of SWC
294 and R_S depend on the effective snow density. The estimates of D_m and N_w can be achieved in a
295 similar way. It is worth mentioning again that snow attenuations, though correctable, are
296 typically negligibly small for most Ku- and Ka-band spaceborne radar measurements.

297

298 As LUTs change with different scattering models and PSD parameterizations, a proper selection
299 of the tables is critical to the accuracy of the retrieval. It is instructive to conduct a sensitivity
300 study with respect to the model assumptions and to gain an understanding of the uncertainties
301 associated with each of the models. Figure 7 provides such a sensitivity study in which the LUTs
302 are checked against 3 μ values. Similar to the findings in Fig.4, a change in μ leads to changes in
303 the estimates of SWC and R_S of less than 20% so that the assumption of μ equal to zero, as found

304 in many observations, yields a reasonable approximation for the estimates of snow. Although it
305 is worth testing the scattering databases of the aggregates formed from various crystal habits, it is
306 not the focus of the study to evaluate and validate these scattering databases. Because the mass
307 of the aggregates is the dominant factor in the scattering parameters at Ku- and Ka-bands,
308 significant differences among the various scattering databases are not expected. This is
309 evidenced by the fact of that there is good agreement between the scattering databases derived by
310 Nowell et al. (2013) and Kuo et al. (2016) and that the small variations of the scattering and
311 extinction coefficients as computed from various aggregate models (Kuo et al. 2016) can be seen
312 from the variations in the data (blue) shown in Figs.2-3.

313

314 **3 Assessment of snow retrieval: PSD model assumptions**

315

316 Because of the complexity of snowfall processes and the difficulties encountered in accurately
317 measuring the microphysical properties, validating snow estimates is a challenging task. With the
318 advent of more advanced digital cameras and image processing technologies, measurements of
319 falling snow have been improved to the point where the snow particle size spectra and fall
320 velocities can be obtained fairly accurately (Bohm 1989; Huang et al. 2010 and 2015; Garrett et
321 al. 2012). An independent and direct measurement of the mass of individual snow particles is,
322 however, still a difficult task, and therefore direct measurements of the snow mass spectrum are
323 rarely available. Several investigations into deriving snow mass spectra are being pursued, which
324 are in fact part of the effort in the GPM ground validation project. These methods are based on
325 the principle that particle masses can be related to their fall velocities after accounting for air
326 drag and other aerodynamics effects (Bohm 1989; Heymsfield et al. 2010). Understanding the
327 microphysical properties of snow should further improve our ability to generate better scattering

328 representations and more accurate look-up tables for retrieving snow bulk properties from the
329 DPR. It would be ideal to evaluate snow retrievals with co-located dual-wavelength radar
330 measurements and in situ snow microphysical measurements. These data, though desirable, are
331 not available. Our attention is therefore focused on the assessment of the PSD assumptions used
332 in developing the retrieval algorithms using measured PSD.

333 To check the consistency of snow retrievals using the LUTs, measurements of snow spectra are
334 used. The data were obtained from 8 snow events during winter of 2014 taken at the NASA
335 Wallops Flight Facility in Wallops Island, Virginia using the Snow Video Imager/Particle Image
336 Probe (SVI/PIP). Table 1 provides details of these events that include starting and ending times
337 of snowfall, mean temperature as well as total accumulations of each event. In Wallops Island
338 annual mean snowfall is about 200.66 mm, and in 2014 it was recorded to be 223.66 mm,
339 slightly more than average. Although the PIP measures the dimensions or sizes of the
340 snowflakes and their fall velocities, it does not provide measurements of particle mass. In order
341 to compute the radar reflectivities and snow bulk parameters as in (4) and (5), the mass spectra or
342 melted size spectra are needed. Conversion of the PSD measurements to the mass spectra,
343 however, relies on the empirical mass-size relations. There are many such relationships available
344 in the literature that can be used to derive $m(D)$ (Nakaya 1954; Magono and Nakamura 1965;
345 Zikmund and Vali 1972; Locatelli and Hobbs 1974; Mitchell et al. 1990; Brandes et al. 2007;
346 Heymsfield et al. 2010). These results show some variability depending on snow type, amount of
347 riming and other conditions under which the measurements were made. In this study, two well-
348 known mass-size relations, the results from Heymsfield et al. (2010) and Brandes et al. (2007),
349 are used to test how the estimates of snow change with use of different mass-size relations when
350 the same LUTs are used.

351

352 An example of the PSD measurements is shown in Fig.8, in which $N(D)$ of the PSD (top), shown
353 along the vertical with the amplitude of the spectrum given by the color scale, is given as a
354 function of time. The equivalent snowfall rate (R_s) (middle) and median mass diameter (D_m) (bottom)
355 are also shown for the same time period. For the computations of snowfall rate and D_m , empirical
356 snow mass-size relations are used in conjunction with the measured snow particle size spectra
357 and fall velocities. The following equations are used for obtaining R_s and D_m :

358

$$D_m = \frac{\int_0^\infty D m(D)N(D)dD}{\int_0^\infty m(D)N(D)dD}, \quad (4)$$

359

$$R_s = \frac{36 \times 10^{-4}}{\rho_w} \int_{D_{min}}^{D_{max}} N(D) m(D)V(D)dD, \quad (5)$$

360 where D and D_m in (4) and (5) as well as in Fig.8 are, respectively, the actual particle diameter
361 and median mass diameter rather than the melted sizes employed in the rest of the paper. $m(D)$
362 is the particle mass-size relation, and ρ_w is the water mass density taken to be 1 g/cm^3 . Note also
363 that the data shown in Fig. 8 represent a measurement period of 1000 minutes of snow data
364 (~three snow events) with a one-minute integration time. The mass-size relation of Heymsfield et
365 al. (2010) is used for computations of R_s and D_m .

366

367 Illustrated in Fig.9 are the scatter plots (red dots) of SWC (top row) and R_s (bottom row)
368 computed from the measured PSD with use of mass-size relations when the hybrid scattering
369 tables are assumed. For reference, the LUTs derived from the constant effective density
370 scattering models as shown in Fig.6 are superimposed in Fig.9. The SWC and R_s as well as the
371 quantities associated with the Ku- and Ka-band radar reflectivities shown in Fig.9 are obtained
372 from a total of about 8000 1-minute PSD measurements collected from the PIP during the winter

373 of 2014 at Wallops using the mass-size relations of Brandes et al. (left column) and Heymsfield
374 et al. (right column). Mass-size relations are used to convert the measured particle size
375 distribution (PSD) to the melted size distribution from which the scatterings and snow bulk
376 parameters can be computed as in (2)-(5). The mass-size relations used in Fig.9 are those from
377 Eq.(8) of Brandes et al. (2007) and Eq.(10) of Heymsfield et al. (2010). The procedures used in
378 obtaining the radar parameters and SWC and R_s from the measured PSD are shown in the flow
379 diagram of Fig.10. Analysis of the SWC results indicates that the snow water content derived
380 from the measured PSD agree reasonably well with those from the tables when the effective
381 snow density is taken to be 0.2 g/cm^3 . Because the scattering table, which is a hybrid formed
382 from the mean aggregate solution at small particle sizes with the spheroidal particle model at
383 larger sizes, used for computing the reflectivities of the measured PSD and the scattering results
384 with a density of 0.2 g/cm^3 are nearly the same as shown in Figs.2-3, the differences in snow
385 water content between the measured PSD and the table results from a density of 0.2 g/cm^3 are
386 mostly caused by the differences between measured and modeled melted particle size
387 distributions. As noted earlier, the exponential melted-size distribution is assumed in the look-up
388 tables while the measured melted-size distribution is derived from the measured particle diameter
389 spectrum and the mass-size relation that generally will be different from an exponential
390 distribution. Computation of the snowfall rate, on the other hand, depends not only on the
391 particle mass (or melted-size) spectrum but also on the particle fall velocities. Most of the
392 estimated snowfall rates, as derived from the measured PSD and the mass-size relations, and
393 shown in the lower panels of Fig.9, lie between the table results with effective densities of 0.1
394 and 0.2 g/cm^3 . The mean differences of the SWC between the 0.2 g/cm^3 snow density LUTs and
395 the PSD-derived results are about 20% for Ku-band radar reflectivities greater than 15 dBZ (the

396 approximate minimum detectable signal of the DPR Ku-band channel). Larger differences
397 between the R_s estimates are found, and can be attributed to differences in the snow fall velocity
398 spectra between the measured and modeled mass distribution. The terminal velocities of
399 snowflakes used for the computations of the LUTs are based on the results of Magono and
400 Nakamura (1965) while the measured fall velocities are used for the computations of PSD
401 snowfall rate.

402

403 The overall agreement of the snow water content between the results from the measured PSD
404 and the results from the LUTs suggests that the exponential particle distribution model assumed
405 in the tables is reasonable. Different mass-size relations lead to different mass spectra for a given
406 measured PSD. That the retrieval results from the Brandes et al. and Heymsfield et al. mass-size
407 relations follow the trends of SWC and R_s similar to those derived from the LUTs further
408 suggest that the Ku- and Ka-band dual-wavelength techniques adopted are relatively insensitive
409 to the choice of either the Brandes or the Heymsfield mass-size relation. These results
410 approximately yield the table values obtained from the 0.2 g/cm^3 snow density. It is also worth
411 mentioning that the results from the measured PSD are relatively insensitive to PSD integration time even
412 though the scatter in the data is slightly reduced if a longer integration is used.

413

414 **4 Summary**

415

416 The ultimate goal of this study is to better understand the estimation process in retrieving snow
417 microphysical properties (N_w and D_m) and the associated bulk parameters (SWC and R_s) for
418 improvement of the Ku- and Ka-band dual frequency radar retrieval. This is done by first finding
419 suitable single scattering tables and PSD models and then using this information to construct

420 snow retrieval look-up tables. Presently available scattering databases, though accurate and
421 useful, are limited to small and moderate particle sizes. To extend the results to larger sizes, a
422 simple scattering model that agrees well with the scattering databases at small particle sizes is
423 used. It is found that a snow particle model consisting of randomly oriented oblate spheroids
424 with an effective mass density of 0.2 g/cm^3 yields good agreement with the results from the
425 scattering databases at Ku- and Ka-band. Thus the single-particle scattering database is a hybrid
426 that uses the scattering database for small and moderate particles and a simple randomly oriented
427 oblate with a constant effective mass density of 0.2 g/cm^3 for large particles.

428

429 Using single scattering tables and an assumed PSD model, the Ku- and Ka-band radar
430 reflectivity factors and snow bulk parameters are computed. Thus, the relationships between the
431 results of DFR and SWC and R_s are established to form the dual-wavelength radar retrieval look-
432 up tables. Retrievals of snow water content and snowfall rate, as the primary focus of this study,
433 are therefore achieved by using newly introduced look-up tables that directly link Ku- and Ka-
434 band radar reflectivities to hydrometeor parameters without the use of derived PSD parameters.
435 The look-up tables are formed so that SWC and R_s , both of which are normalized by the Ku-
436 band radar reflectivity factor, are expressed as a function of the differential frequency ratio of
437 Ku- and Ka-bands. The look-up tables offer not only computational advantages but provide
438 direct insight into how the model assumptions impact the retrieval results. The nature of one-to-
439 one relations between the normalized hydrometeor parameters and DFR provides a means to
440 obtain unique solutions of the snow parameters for a given PSD and single scattering model. To
441 understand the uncertainties in the snow estimates associated with the PSD parameterizations
442 and scattering models, a sensitivity study was done, finding that the choice of shape factor of the

443 gamma PSD has only a slight impact on the retrievals. As such, a value of μ of zero, as
444 supported by some observations, should yield reasonable estimates of snow parameters from the
445 perspective of dual-wavelength radar retrieval.

446

447 Self-consistency of the snow retrievals has been checked using measurements of snow PSD and
448 fall velocity acquired from the PIP during the winter of 2014 in Wallops. Among several
449 assumptions that have been examined are conversions to particle mass spectra using different
450 mass-size relations, scattering particle models and snow PSD. Analysis of nearly 8000 1-minute
451 PSD measurements suggests that exponential PSD model ($\mu=0$) is sufficiently accurate for the
452 dual-wavelength radar retrieval of snow bulk parameters. It also indicates that the use of either
453 the Heymsfield or the Brandes mass-size relation yields approximately the same snow estimates.
454 However, these findings should be viewed as preliminary because of the limited data
455 measurements at a single location. Collections of long-term PSD data, fall velocities and
456 information on particle mass spectra at multiple sites will provide further evaluation of the
457 performance of the Ku- and Ka-band radar techniques. Further tests of the scattering tables will
458 be done by comparing the accuracy of the simple particle model against scattering results from
459 larger simulated aggregates, as these results become available.

460

461 **ACKNOWLEDGEMENTS:** This work is supported by Dr. R. Kakar of NASA Headquarters
462 under NASA's Precipitation Measurement Mission (PMM) Grant NNH12ZDA001N-PMM. The
463 authors also wish to thank Mr. Jorel Torres of South Dakota School of Mines & Technology for
464 providing and processing SVI/PIP data, and Dr. Kwo-Sen Kuo of University of Maryland for
465 providing the scattering database.

467

Appendix

468

List of Symbols and Acronyms

469	GPM:	Global Precipitation Measurement
470	DPR:	Dual-frequency Precipitation Radar
471	NASA:	National Aeronautics and Space Administration
472	JAXA:	Japan Aerospace Exploration Agency
473	Ku-band:	Frequency of 13.6 GHz
474	Ka-band:	Frequency of 35.6 GHz
475	PSD:	Particle Size Distribution
476	SVI/PIP:	Snow Video Imager/Particle Image Probe
477	DDA:	Discrete Dipole Approximation
478	$N(D)$:	Particle Size Distribution
479	N_w :	Scale Factor of Particle Size Distribution
480	μ :	Shape Factor of Gamma Distribution
481	D :	Particle Diameter
482	D_m :	Mass-weighted Diameter
483	Λ :	Slope Parameter
484	DFR:	Differential Frequency Ratio
485	SWC:	Snow Water Content
486	R_s :	Equivalent Snowfall Rate
487	LUT:	Look-up Table
488	Z_{Ku} :	Ku-band Radar Reflectivity Factor
489	Z_{Ka} :	Ka-band Radar Reflectivity Factor
490	$m(D)$:	Particle Mass as Function of Particle Diameter
491	$V(D)$:	Particle Fall Velocity
492	ρ_w :	Liquid Mass Density
493	ρ_s :	Snow Mass Density
494	D_{min} :	Minimum Diameter
495	D_{max} :	Maximum Diameter
496	f :	Frequency
497	γ :	Aspect Ratio of Particle
498		

499

500 **References**

501 Brandes, E., K. Ikeda, G. Zhang, M. Schoenhuber, and R. Rasmussen, 2007: A statistical and
502 physical description of hydrometeor distributions in Colorado snowstorms using a video
503 distrometer. *J. Appl. Meteor. Climat.*, **46**, 634-650.

504

505 Bohm, H.P., 1989: A general equation for the terminal fall speed of solid hydrometeors. *J.*
506 *Atmos. Sci.*, **46**, pp. 2419-2427.

507

508 Botta, G., K. Aydin, and J. Verlinde, 2010: Modeling of microwave scattering from cloud ice
509 crystal aggregates and melting aggregates: A new approach. *IEEE Geo. Rem. Sens. Lett.*, **7**,
510 572-576.

511

512 Botta, G., K. Aydin, J. Verlinde, A.E. Avramov, A.S. Ackerman, A.M. Fridlind, G.M.
513 McFarquhar and M. Wolde, 2011: Millimeter wave scattering from ice crystal aggregates:
514 Comparing cloud model simulations with X- and Ka-band radar measurements. *J. Geophys.*
515 *Res.*, **116**, D00T04.

516

517 Botta, G., K. Aydin, and J. Verlinde, 2013: Variability in millimeter wave scattering properties
518 of dendritic ice crystals. *J. Quant. Spectrosc. Radiat. Transf.*, **131**, 105-104.

519

520 Bringi, V., G. Huang, V. Chandrasekar and E. Gorgucci, 2002: A methodology for estimating the
521 parameters of a Gamma raindrop size distribution model from polarimetric radar data:
522 Application to a squall-line event from the TRMM/Brazil campaign. *J. Oceanic and Atmos.*
523 *Tech.*, **19**, 633-645.

524

525 Draine, B. T., and P. J. Flatau, 1994: Discrete dipole approximation for scattering calculations. *J.*
526 *Opt. Soc. Am. A.*, **11**, 1491-1499.

527

528 Garrett, T. J., Fallgatter, C., Shkurko, K., and Howlett, D., 2012: Fall speed measurement and
529 high-resolution multi-angle photography of hydrometeors in free fall. *Atmos. Meas. Tech.*, **5**,
530 2625-2633.

531

532 Gorgucci, G. Scarchilli, V. Chandrasekar and V. Bringi, 2000: Measurement of mean raindrop
533 shape from polarimetric radar observations. *J. Atmos. Sci.*, **57**, 3406-3413.

534

535 Gorgucci, E., G. Scarchilli, V. Chandrasekar, and V. Bringi, 2002: Estimation of raindrop size
536 distribution parameters from polarimetric radar measurements. *J. Atmos. Sci.*, **59**, 2373-
537 2384.

538

539 Gravner, J., and D. Griffeath, 2009: Modeling of snow-crystal growth: A three dimensional
540 mesoscopic approach. *Phys. Rev. E*, **79**, 011601.

541

542 Gunn, K. L. S., and J.S. Marshall, 1958: The distribution with size of aggregate snowflakes. *J.*
543 *Meteor.*, **15**, 452-461.

544

545 Heymsfield, A. J., Z. Wang, and S. Matrosov, 2005: Improved radar ice water content retrieval
546 algorithms using coincident microphysical and radar measurements. *J. Appl. Meteor.*, **44**,
547 1391–1412.

548

549 Heymsfield, A. J., and C. D. Westbrook, 2010: Advances in the estimation of ice particle fall
550 speeds using laboratory and field measurements. *J. Atmos. Sci.*, **67**, 2469–2482.

551

552 Heymsfield, A. J., C. Schmitt, A. Bansemer, and C. H. Twohy, 2010: Improved representation of
553 ice particle masses based on observations in natural clouds. *J. Atmos. Sci.*, **67**, 3303–3318.

554

555 Hogan, R., A. Illingworth, and H. Sauvageot, 2000: Measuring crystal size in cirrus using 35-
556 and 94-GHz radars. *J. Atmos. Oceanic Technol.*, **17**, 27-37.

557

558 Hou, A., G. S. Jackson, C. Kummerow, and C. M. Shepherd, 2008: Global precipitation
559 measurement. *Precipitation: Advances in Measurement, Estimation, and Prediction*, S.
560 Michaelides, Ed., Springer, 131–169.

561

562 Hou, A. Y., R. K. Kakar, S. Neeck, A. A. Azarbarzin, C. D. Kummerow, M. Kojima, R. Oki, K.
563 Nakamura, and T. Iguchi, 2014: The global precipitation measurement mission. *Bull.
564 American Meteor. Soc.*, **95**, 701-722.

565

566 Huang, G., Bringi, V. N., Cifelli, R., Hudak, D. and Petersen, W. A., 2010: A Methodology to
567 Derive Radar Reflectivity–Liquid Equivalent Snow Rate Relations Using C-Band Radar and
568 a 2D Video Disdrometer. *J. Atmos. Oceanic Technol.*, **27**, 637-651.

569

570 Huang, G., V.N. Bringi, D. Moisseev, W.A. Petersen, L. Bliven and D. Hudak, 2015: Use of 2D-
571 video disdrometer to derive mean density–size and Ze–SR relations: Four snow cases from
572 the light precipitation validation experiment, *Atmos. Res.*, **153**, 34–48.

573

574 Kuo, K-S, W. S. Olson, B. T. Johnson, M. Grecu, L. Tian, T. L. Clune, B. H. van Aartsen, A. J.
575 Heymsfield, L. Liao, and R. Meneghini, 2016: The microwave radiative properties of falling
576 snow derived from realistic ice particle models. Part I: An extensive database of simulated
577 pristine crystals and aggregate particles, and their scattering properties. *J. Appl. Meteorol.
578 Climatol.*, **55**, 691-708.

579

580 Liao, L., R. Meneghini, H. Nowell and G. Liu, 2013: Scattering computations of snow aggregates
581 from simple geometrical particle models. *IEEE J. Selected Topics in Earth Obs. and Remote
582 Sens.*, **6**, 1409-1417.

583

584 Liu, G., 2004: Approximation of single scattering properties of ice and snow particles for high
585 microwave frequencies. *J. Atmos. Sci.*, **61**, 2441-2456.

586

587 Liu, G., 2008: A database of microwave single-scattering properties for non spherical ice
588 particles. *Bull. Am. Meteorol. Soc.*, **89**, 1563-1570.

589

590 Locatelli, J., and P. Hobbs, 1974: Fall speeds and masses of solid precipitation particles. *J.
591 Geophys. Res.*, **79**, 2185-2197.

592

593 Magono C., and T. Nakamura, 1965: Aerodynamic studies of falling snowflakes, *J. Meteorol.
594 Soc. Jpn.*, **43**, 139–147.

595

596 Matrosov, S. Y., 1998: A dual-wavelength radar method to measure snowfall rate. *J. Appl.
597 Meteor.*, **37**, 1510–1521.

598

599 Matrosov, S. Y., A. J. Heymsfield, and Z. Wang, 2005: Dual-frequency ratio of non-spherical
600 atmospheric hydrometeors. *Geophys. Res. Lett.*, **32**, L13816, doi:10.1029/2005GL023210.

601

602 Mitchell, D. L., R. Zhang, and R. L. Pitter, 1990: Mass-dimensional relations for ice particles
603 and the influence of riming on snowfall rates. *J. Appl. Meteor.*, **29**, 153-163.

604

605 Nakaya, U., 1954: *Snow Crystals: Natural and Artificial*. Harvard University Press, 510pp.

606

607 Newman, A., P. A. Kucera, and L. Bliven, 2009: Presenting the snow video imager. *J. Atmos.
608 Ocean. Technol.*, **26**, 167-179.

609

610 Nowell, H., G. Liu, and R. Honeyager, 2013: Modeling the microwave single-scattering
611 properties of aggregate snowflakes. *J. Geophys. Res. Atmos.*, **118**, 7873–7885.
612 doi:10.1002/jgrd.50620.

613

614 Petty, G. W., and W. Huang, 2010: Microwave backscattering and extinction by soft ice spheres
615 and complex snow aggregates. *J. Atmos. Sci.*, **67**, pp. 769-787.

616

617 Seto, S., T. Iguchi, and T. Oki, 2013: The basic performance of a precipitation retrieval algorithm
618 for the global precipitation measurement mission's single/dual-frequency radar
619 measurements. *IEEE Trans. Geosci. Remote Sens.*, **51**, 5239–5251.

620

621 Szyrmer, W., and I. Zawadzki, 2014a: Snow studies. Part III: Theoretical derivations for the
622 ensemble retrieval of snow microphysics from dual-wavelength vertically pointing radars. *J.
623 Atmos. Sci.*, **71**, 1158–1170.

624

625 Szyrmer, W., and I. Zawadzki, 2014b: Snow studies. Part IV: Ensemble retrieval of snow
626 microphysics from dual-wavelength vertically pointing radars. *J. Atmos. Sci.*, **71**, 1172–1186.

627

628 Wang, Z., G. M. Heymsfield, L. Li, and A. J. Heymsfield, 2005: Retrieving optically thick ice
629 cloud microphysical properties by using airborne dual-wavelength radar measurements. *J.
630 Geophys. Res.*, **110**, D19201, doi:10.1029/2005JD005969.

631

632 Weinman, J., and M.-J. Kim, 2007: A simple model of the millimeter-wave scattering parameters
633 of randomly oriented aggregates of finite cylindrical ice hydrometeors. *J. Atmos. Sci.*, **64**,
634 634-644.

635

636 Zikmund, J., and G. Vali, 1972: Fall patterns and fall velocities of rimed ice crystals. *J. Atmos.*
637 *Sci.*, **29**, 1334-1347.
638

639 Table 1 Snow events during winter of 2014 in Wallops Island, Virginia

640

Events	Start Time (UTC)	End Time (UTC)	Accumulation (mm)	Mean Temperature (°C)
1	JAN03 05:09	JAN03 11:30	46.41	-1.4
2	JAN21 22:05	JAN22 10:03	5.52	-5.4
3	JAN28 20:41	JAN29 12:40	62.12	-9.5
4	FEB14 01:58	FEB14 05:12	6.37	1.9
5	FEB15 20:41	FEB15 23:23	0.76	2.2
6	MAR03 14:40	MAR03 22:00	34.15	-4.4
7	MAR17 08:04	MAR17 20:53	20.93	0.8
8	MAR25 18:50	MAR26 06:13	47.40	1.0

641

642 Figure captions:

643 Fig.1 Comparisons of backscattering (left) and extinction (right) coefficients of 3 snow
 644 aggregates with the results from the sphere, oblate and prolate spheroids at a frequency of 35.6
 645 GHz in terms of equivalent ice diameter. A constant snow density of 0.2 g/cm³ is assumed for all
 646 spherical and spheroidal particle models. The oblate and prolate spheroids are randomly oriented
 647 with aspect ratios (γ) of 0.5 and 2, respectively.

648 Fig.2 Backscattering (left) and extinction (right) coefficients from the scattering database (blue
 649 dots), simple scattering model (red curves), which is the randomly-oriented oblate spheroid with
 650 a constant effective density of 0.2 g/cm³ and an aspect ratio of 0.7, and scattering-database-
 651 simple-model-combined results (black curves), also referred to as “fitted”, at Ku band. The mean
 652 values of the scattering results are used for the combined results over the data range.

653 Fig.3 Backscattering (left) and extinction (right) coefficients from the scattering database (blue
 654 dots), simple scattering model (red curves), which is the randomly-oriented oblate spheroid with
 655 a constant effective density of 0.2 g/cm³ and an aspect ratio of 0.7, and scattering-database-
 656 simple-model-combined results (black curves), also referred to as “fitted”, at Ka band. The mean
 657 values of the scattering results are used for the combined results over the data range.

658 Fig.4 The differential frequency ratio ($DFR=10\log_{10}(Z_{Ku}/Z_{Ka})$) as a function of equivalent-
 659 liquid median mass diameter D_m . (Left): DFR- D_m relations are plotted with several effective
 660 snow densities (ρ_s) from 0.1 to 0.4 g/cm³ as the shape factor (μ) of the gamma PSD is set to zero
 661 and the aspect ratio (γ) of the oblate spheroid particles is set to 0.7. (Middle): DFR- D_m relations
 662 are plotted with the aspect ratios of 0.5, 0.7 and 1 at $\rho_s=0.2$ g/cm³ and $\mu=0$. (Right): DFR- D_m
 663 relations are plotted with the values of μ of 0, 3 and 6 at $\rho_s=0.2$ g/cm³ and $\gamma=0.7$.

664 Fig.5 The retrieval look-up tables that show the snow water content (SWC) (top-left) and
 665 equivalent snowfall rate (R_s) (top-right), both of which are normalized by the Ku-band radar
 666 reflectivity factor (Z_{Ku}), as a function of the DFR, defined by $10\log_{10}(Z_{Ku}/Z_{Ka})$, for several
 667 effective snow densities (ρ_s) with the values from 0.05 to 0.5 g/cm³. The liquid equivalent
 668 median mass diameter D_m (bottom-left) and the PSD scale parameter N_w normalized by Z_{Ku}
 669 (bottom-right) are also plotted in terms of DFR.

670 Fig.6 Flowchart of computing radar parameters and snow size and bulk properties.

671 Fig.7 The look-up tables used for the retrieval of SWC (left) and R_s (right) with μ of 0, 3 and 6,
 672 respectively, as computed from the single scattering tables depicted in Figs.2-3.

673 Fig.8 Example of a segment of the PSD measurements (1000 minutes) in time series taken from
 674 8 snow events during winter of 2014 at the NASA Wallops Flight Facility using the SVI/PIP.
 675 The particle size spectra ($\text{mm}^{-1} \text{m}^{-3}$), shown in the color scale, are given in the top panel while
 676 equivalent snow fall rate and actual median mass diameter are displayed in the middle and

677 bottom panels, respectively. The PSD data, obtained by averaging the measurements over 1-
678 minute integration time, are merged from all the snow events into one data file with consecutive
679 time.

680 Fig.9 The snow water content (SWC) (top row) and equivalent snowfall rate (R_s) (bottom row),
681 both of which are normalized by the Ku-band radar reflectivity factor (Z_{Ku}), as a function of the
682 DFR, defined by $10\log_{10}(Z_{Ku}/Z_{Ka})$, for several effective snow densities (ρ_s) with the values
683 from 0.05 to 0.5 g/cm³. The scatter plots (red dots) are the results derived from the measured
684 PSD that were collected by the SVP/PIP from 8 snow events in the winter of 2014 at the NASA
685 Wallops Flight Facility. Two empirical density-size relationships reported by Brandes et al.
686 (2007) and Heymsfield et al. (2010) are used in converting the measured PSD to the snow mass
687 spectra, and the results from their respective relations are shown in the left and right panels.

688 Fig.10 Flowchart detailing the procedures of obtaining radar reflectivities and snow parameters.

689

690

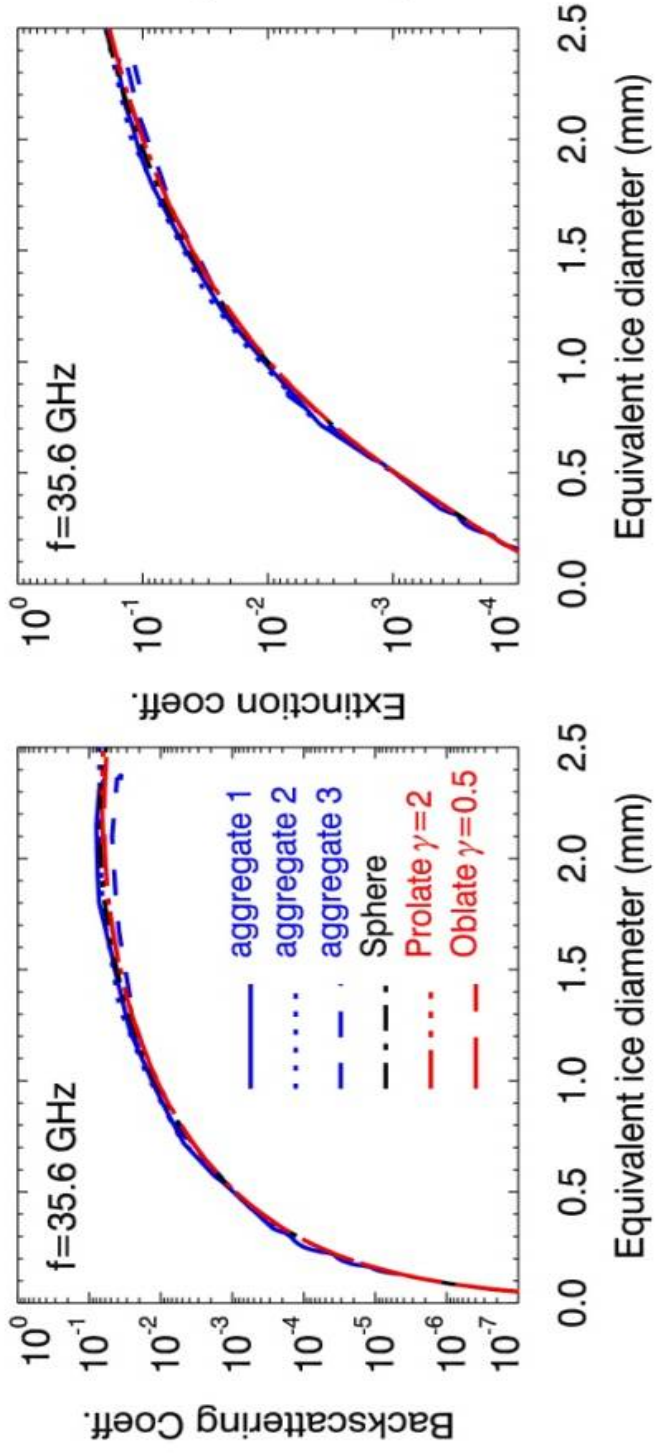


Fig. 1 Comparisons of backscattering (left) and extinction (right) coefficients of 3 snow aggregates with the results from the sphere, oblate and prolate spheroids at a frequency of 35.6 GHz in terms of equivalent ice diameter. A constant snow density of 0.2 g/cm^3 is assumed for all spherical and spheroidal particle models. The oblate and prolate spheroids are randomly oriented with aspect ratios (γ) of 0.5 and 2, respectively.

702

703

704

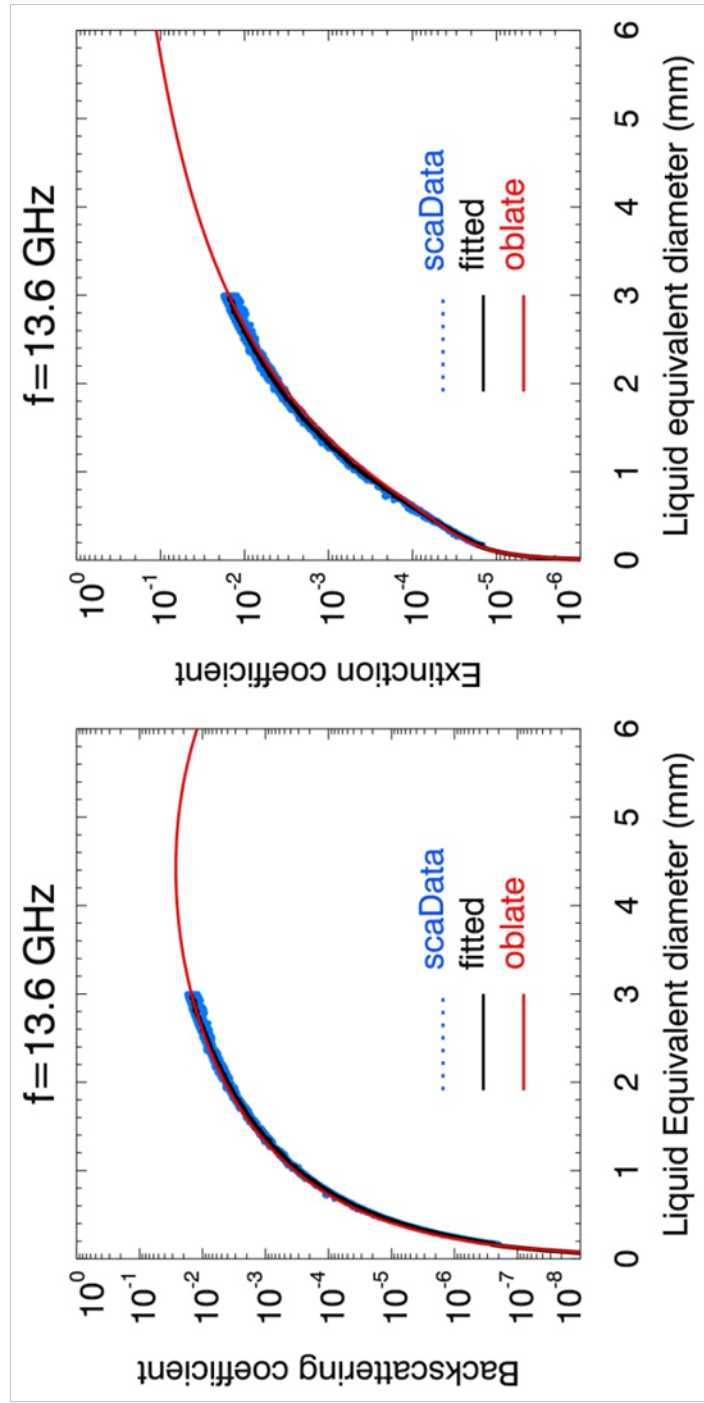


Fig.2 Backscattering (left) and extinction (right) coefficients at Ku-band from the scattering database (blue dots), simple scattering model (red curves), which is the randomly-oriented oblate spheroid with a constant effective density of 0.2 g/cm^3 and an aspect ratio of 0.7, and scattering-database-simple-model-combined results (black curves), also referred to as "fitted". The mean values of the scattering results are used for the combined results over the data range.

705

706
707

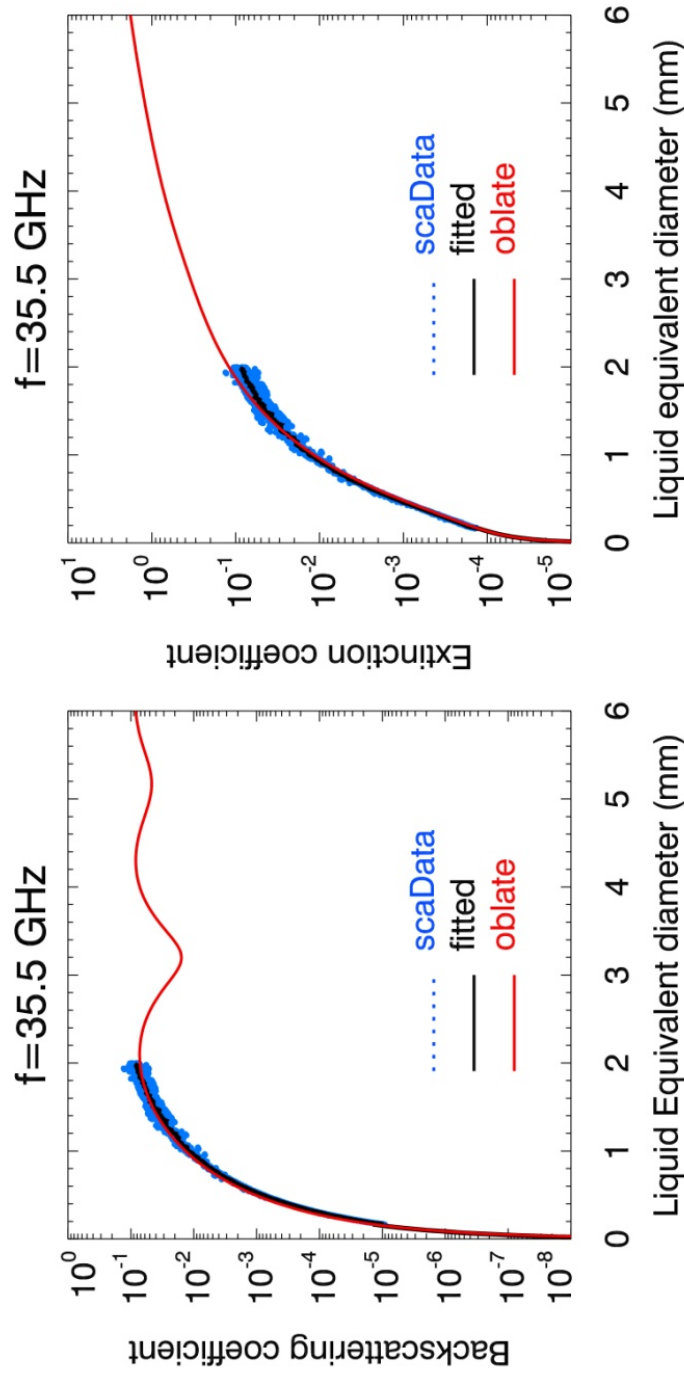


Fig.3 Backscattering (left) and extinction (right) coefficients from the scattering database (blue dots), simple scattering model (red curves), which is the randomly-oriented oblate spheroid with a constant effective density of 0.2 g/cm^3 and an aspect ratio of 0.7, and scattering-database-

708
709
710
711

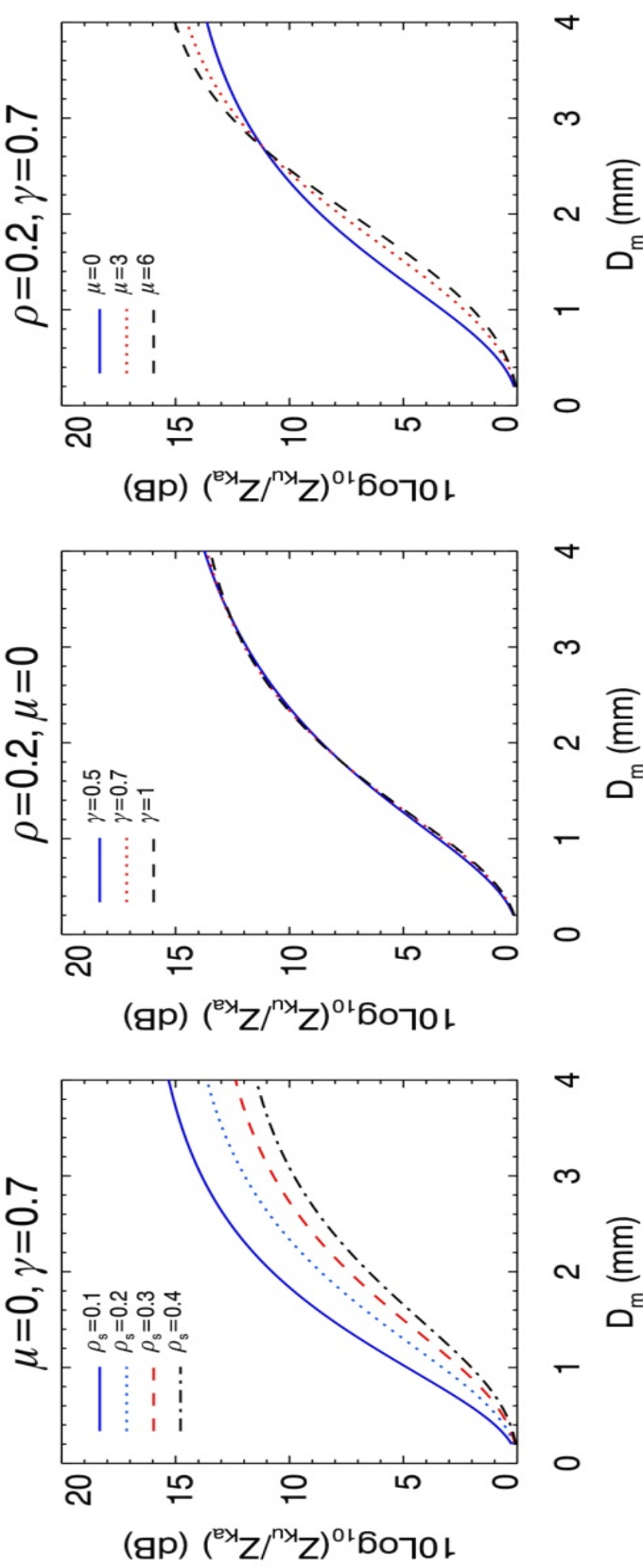
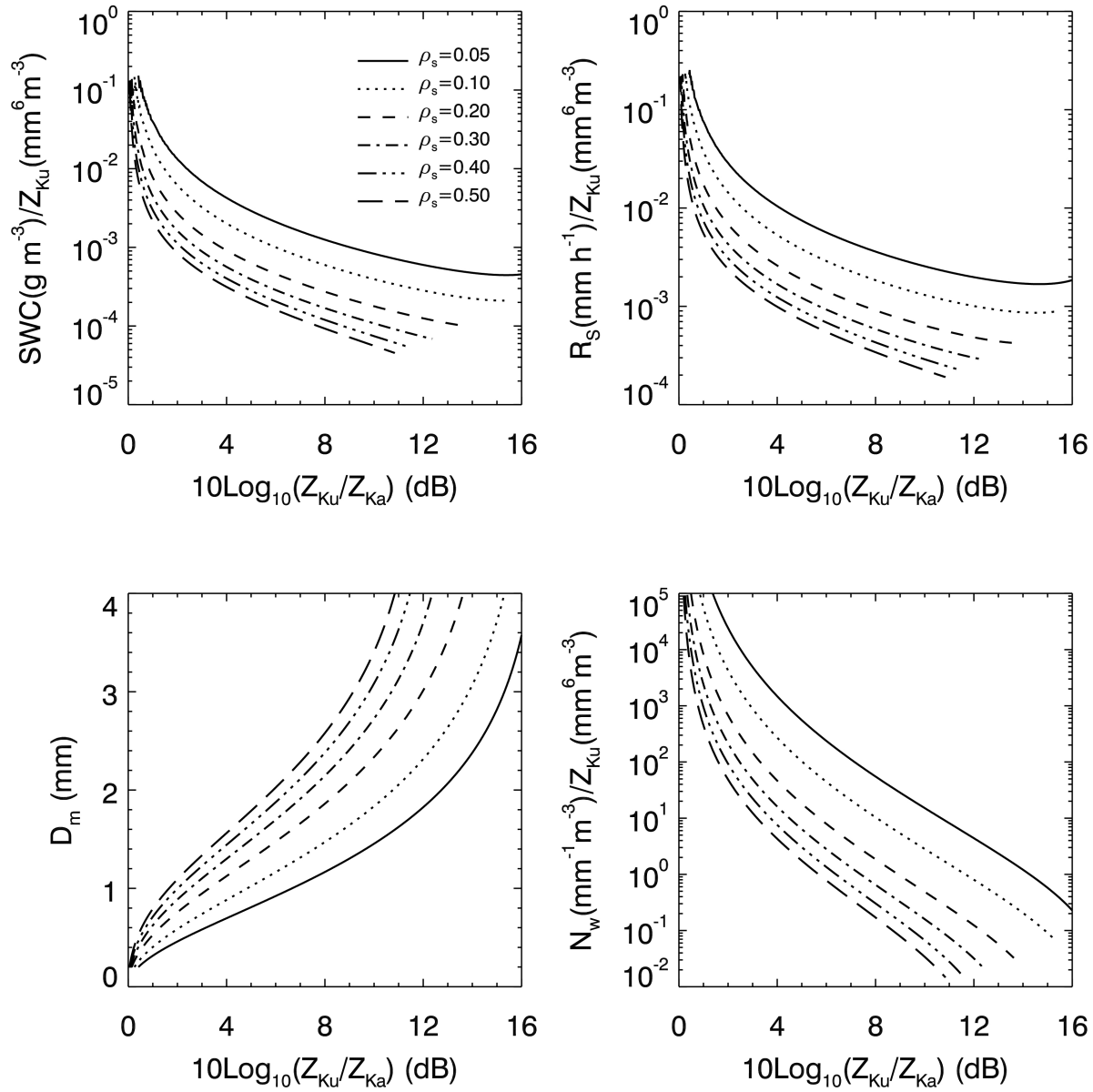


Fig.4 The differential frequency ratio ($DFR=10\log_{10}(Z_{Ku}/Z_{Ka})$) as a function of equivalent-liquid median mass diameter D_m . (Left): DFR- D_m relations are plotted with several effective snow densities (ρ_s) from 0.1 to 0.4 g/cm³ as the shape factor (μ) of the gamma PSD is set to zero and the aspect ratio (γ) of the oblate spheroid particles is set to 0.7. (Middle): DFR- D_m relations are plotted with the aspect ratios of 0.5, 0.7 and 1 at $\rho_s=0.2$ g/cm³ and $\mu=0$. (Right): DFR- D_m relations are plotted with the values of μ of 0, 3 and 6 at $\rho_s=0.2$ g/cm³ and $\gamma=0.7$.



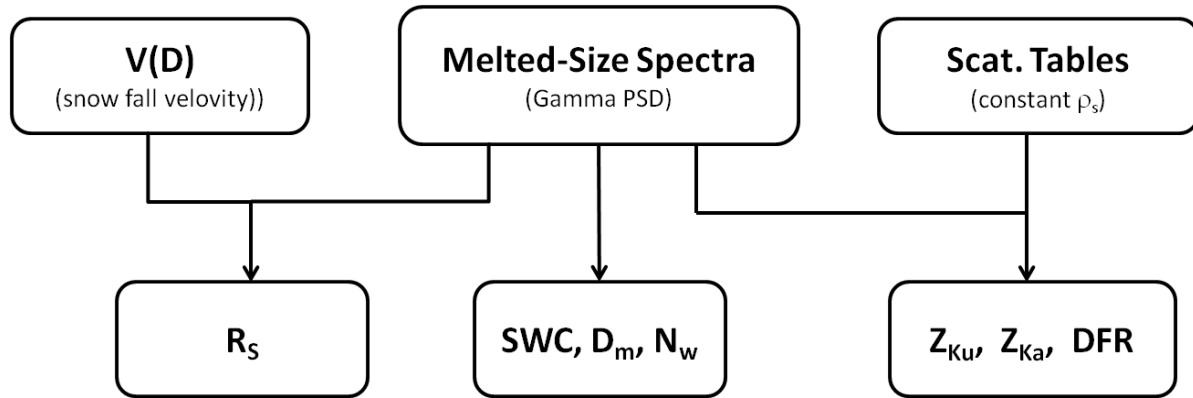
723

724

725

726 Fig.5 The retrieval look-up tables that show the snow water content (SWC) (top-left)
 727 and equivalent snowfall rate (R_s) (top-right), both of which are normalized by the Ku-band radar
 728 reflectivity factor (Z_{Ku}), as a function of the DFR, defined by $10\log_{10}(Z_{\text{Ku}}/Z_{\text{Ka}})$, for several
 729 effective snow densities (ρ_s) with the values from 0.05 to 0.5 g/cm^3 . The liquid equivalent
 730 median mass diameter D_m (bottom-left) and the PSD scale parameter N_w normalized by Z_{Ku}
 731 (bottom-right) are also plotted in terms of DFR.

732

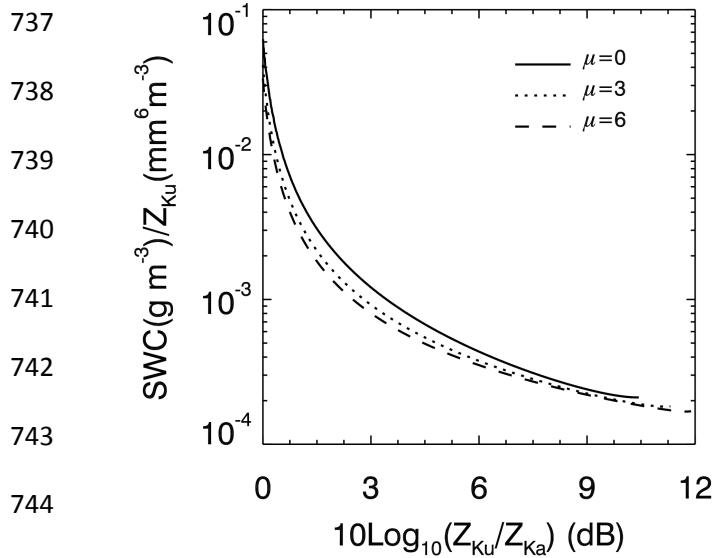


733

734

735 Fig.6 Flowchart of computing radar parameters and snow size and bulk properties.

736



737

738

739

740

741

742

743

744

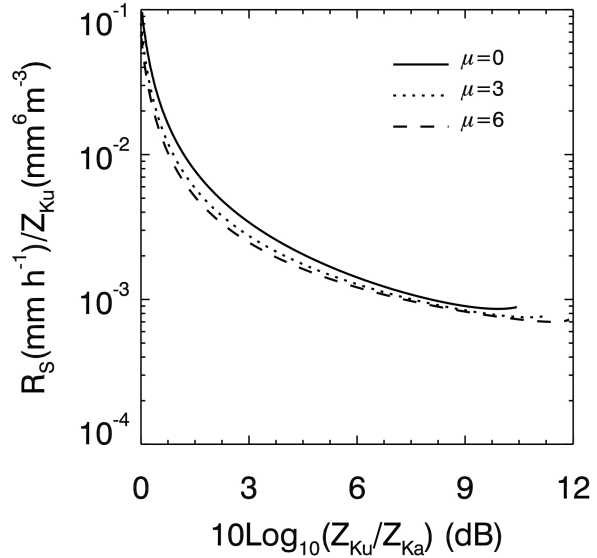
745

746

747

748

749



746

747

748

749

Fig.7 The look-up tables used for the retrieval of SWC (left) and R_s (right) with μ of 0, 3 and 6, respectively, as computed from the single scattering tables depicted in Figs.2-3.

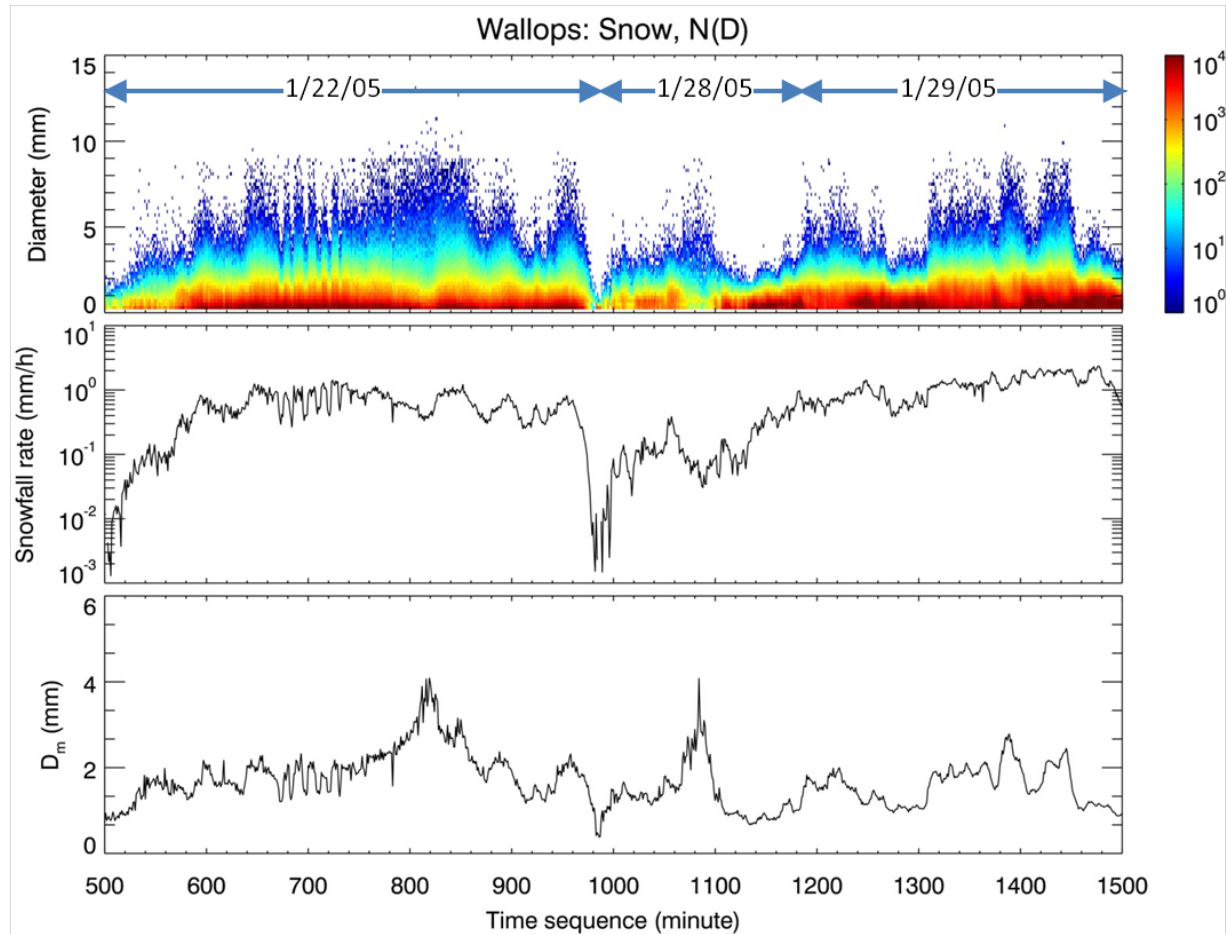
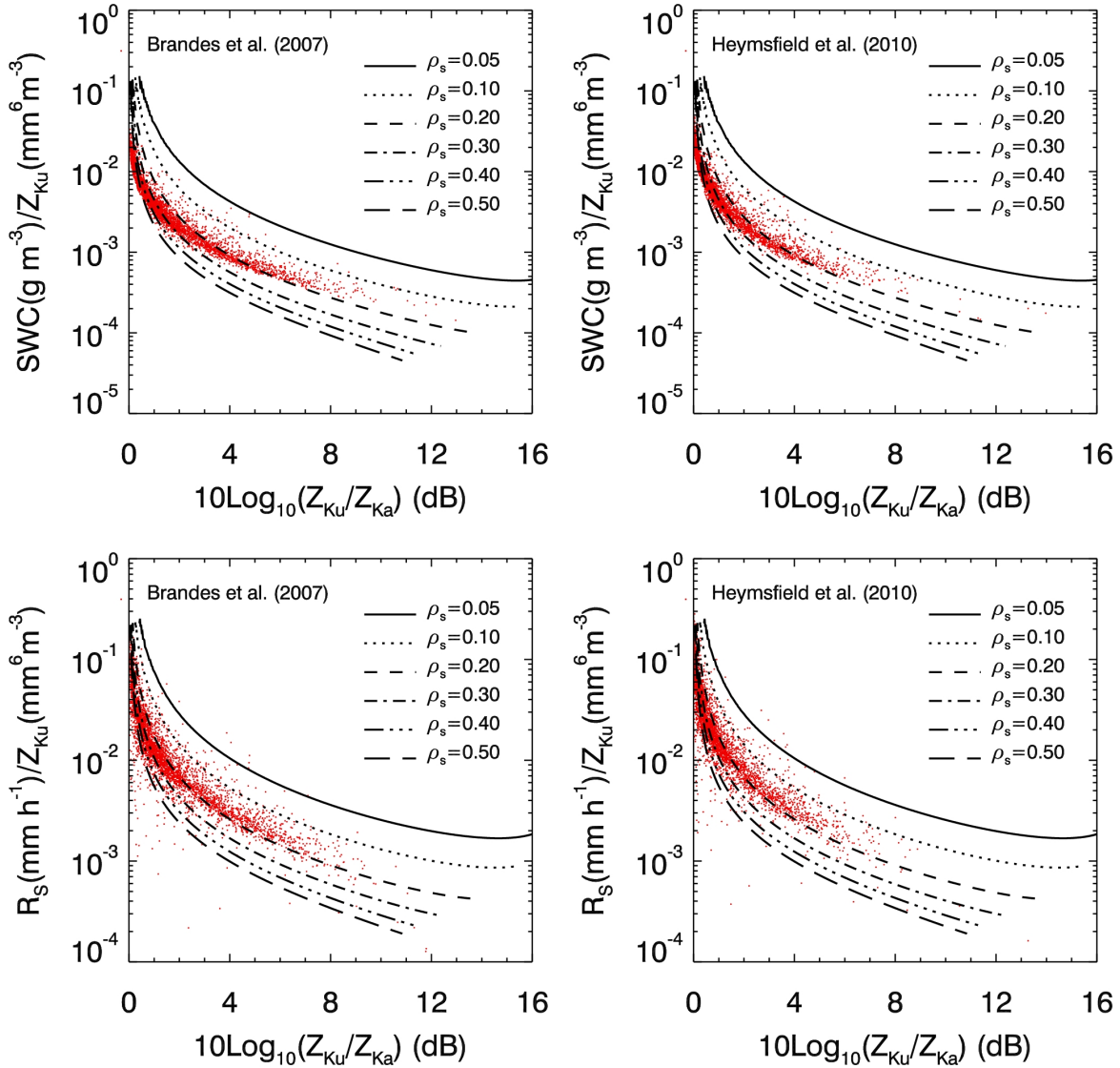


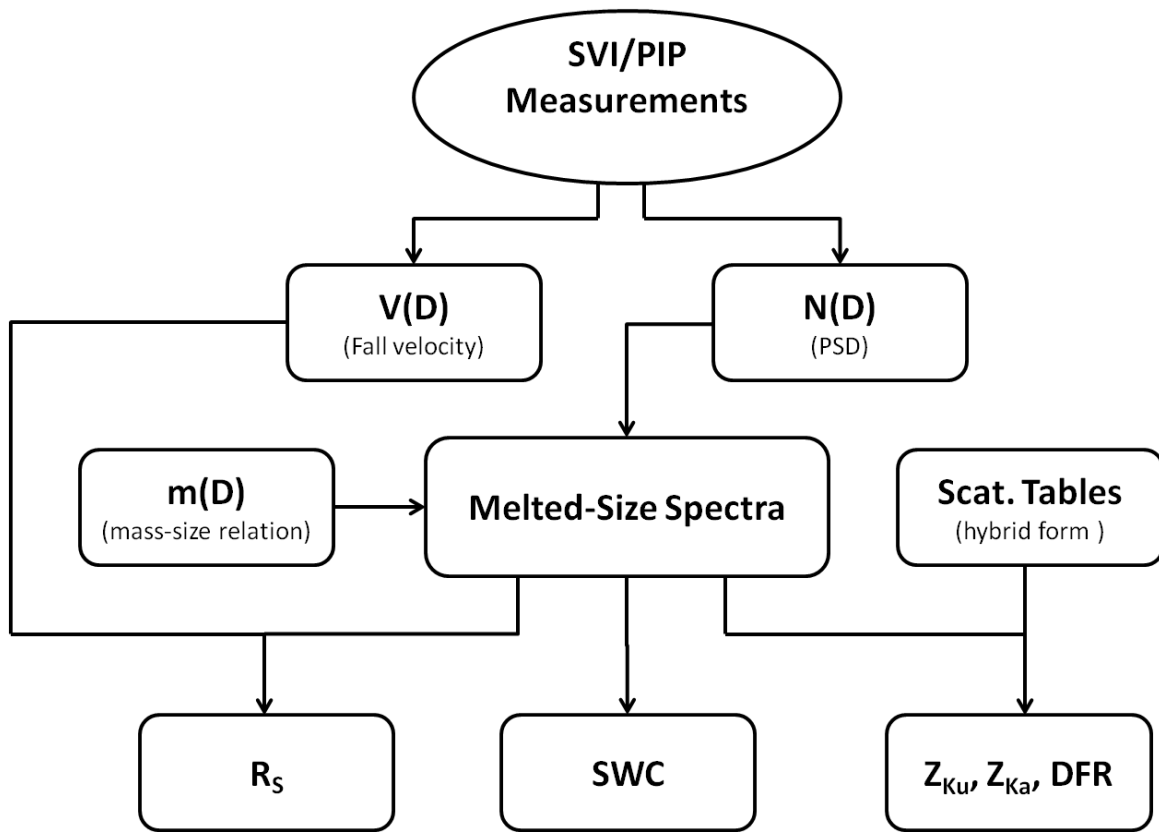
Fig.8 Example of a segment of the PSD data, obtained by averaging the measurements over 1-minute integration time, in time series taken from 8 snow events during winter of 2014 at the NASA Wallops Flight Facility using the SVI/PIP. The particle size spectra ($\text{mm}^{-1} \text{m}^{-3}$), shown in the color scale, are given in the top panel while equivalent snow fall rate and actual median mass diameter are displayed in the middle and bottom panels, respectively. The dates provided in the top panel correspond to the snow events displayed.



758

759 Fig.9 The snow water content (SWC) (top row) and equivalent snowfall rate (R_s) (bottom row),
760 both of which are normalized by the Ku-band radar reflectivity factor (Z_{Ku}), as a function of the
761 DFR, defined by $10\text{LOG}_{10}(Z_{Ku}/Z_{Ka})$, for several effective snow densities (ρ_s) with the values
762 from 0.05 to 0.5 g/cm^3 . The scatter plots (red dots) are the results derived from the measured
763 PSD that were collected by the SVP/PIP from 8 snow events in the winter of 2014 at the NASA
764 Wallops Flight Facility. Two empirical density-size relationships reported by Brandes et al.
765 (2007) and Heymsfield et al. (2010) are used in converting the measured PSD to the snow mass
766 spectra, and the results from their respective relations are shown in the left and right panels.

767



768

769

770 Fig.10 Flowchart detailing the procedures of obtaining radar reflectivities and snow parameters.

771